Bond dissociation energies of FeSi, RuSi, OsSi, CoSi, RhSi, IrSi, NiSi, and PtSi

Andrew Sevy, Erick Tieu, and Michael D. Morse

Articles you may be interested in

Bond dissociation energies of TiC, ZrC, HfC, ThC, NbC, and TaC
The Journal of Chemical Physics **149**, 044306 (2018); 10.1063/1.5041422

Equation-of-motion coupled-cluster theory based on the 4-component Dirac–Coulomb(–Gaunt) Hamiltonian. Energies for single electron detachment, attachment, and electronically excited states
The Journal of Chemical Physics **149**, 174113 (2018); 10.1063/1.5053846

Communication: Can excitation energies be obtained from orbital energies in a correlated orbital theory?
The Journal of Chemical Physics **149**, 131101 (2018); 10.1063/1.5052442

Monte Carlo explicitly correlated many-body Green's function theory
The Journal of Chemical Physics **149**, 174112 (2018); 10.1063/1.5054610

Perturbative treatment of spin-orbit-coupling within spin-free exact two-component theory using equation-of-motion coupled-cluster methods
The Journal of Chemical Physics **148**, 044108 (2018); 10.1063/1.5012041

An atomic mean-field spin-orbit approach within exact two-component theory for a non-perturbative treatment of spin-orbit coupling
The Journal of Chemical Physics **148**, 144108 (2018); 10.1063/1.5023750

Bond dissociation energies of FeSi, RuSi, OsSi, CoSi, RhSi, IrSi, NiSi, and PtSi

Andrew Sevy, Erick Tieu, and Michael D. Morse
Department of Chemistry, University of Utah, Salt Lake City, Utah 84112, USA

Resonant two-photon ionization spectroscopy has been used to investigate the spectra of the diatomic late transition metal silicides, MSi, M = Fe, Ru, Os, Co, Rh, Ir, Ni, and Pt, in the vicinity of the bond dissociation energy. In these molecules, the density of vibronic states is so large that the spectra appear quasicontinuous in this energy range. When the excitation energy exceeds the ground separated atom limit, however, a new decay process becomes available—molecular dissociation. This occurs so rapidly that the molecule falls apart before it can absorb another photon and be ionized. The result is a sharp drop to the baseline in the ion signal, which we identify as occurring at the thermochemical 0 K bond dissociation energy, D_0. On this basis, the measured predissociation thresholds provide D_0 = 2.402(3), 4.132(3), 4.516(3), 2.862(3), 4.169(3), 4.952(3), 3.324(3), and 5.325(9) eV for FeSi, RuSi, OsSi, CoSi, RhSi, IrSi, NiSi, and PtSi, respectively. Using thermochemical cycles, the enthalpies of formation of the gaseous MSi molecules are derived as 627(8), 700(10), 799(10), 595(8), 599(8), 636(10), 553(12), and 497(8) kJ/mol for FeSi, RuSi, OsSi, CoSi, RhSi, IrSi, NiSi, and PtSi, respectively. Likewise, combining these results with other data provides the ionization energies of CoSi and NiSi as 7.49(7) and 7.62(7) eV, respectively. Chemical bonding trends among the diatomic transition metal silicides are discussed. *Published by AIP Publishing.* https://doi.org/10.1063/1.5050934

I. INTRODUCTION

The chemical bond is central to all fields of chemistry, and the strength of the chemical bond is one of the most important means of quantifying the nature of the bond. The bond strength is given by the bond dissociation energy (BDE), which is the 0 K energy required to separate a molecule in its ground vibronic level into fragments in their ground states. For diatomic molecules, the BDE can be directly related to the enthalpy of formation through the thermochemical cycle,

$$\Delta H_{f,0K}(AB(g)) = \Delta H_{f,0K}(A(g)) + \Delta H_{f,0K}(B(g)) - D_0(AB), \quad (1.1)$$

where $\Delta H_{f,0K}(x)$ is the enthalpy of formation of x and $D_0(AB)$ is the BDE of AB. Further information may be obtained through thermochemical cycles that relate the BDE of the neutral molecule to the BDE of the cation (or anion) and the ionization energies (or electron affinities) of the atoms and molecules, as shown in Eqs. (1.2) and (1.3)

$$D_0(A - B) + IE(A) = D_0(A^+ - B) + IE(AB), \quad (1.2)$$

$$D_0(A - B) + EA(AB) = D_0(A^- - B) + EA(A). \quad (1.3)$$

The ionization energies and electron affinities of the atoms are precisely known,[1,2] and the dissociation energies of many diatomic cations have been measured using guided ion beam mass spectrometry (GIBMS) or other techniques.[3–6] Molecular ionization energies may be measured using techniques such as pulsed field ionization zero electron kinetic energy (PFI-ZEKE) spectroscopy,[7–11] and electron affinities may be measured using photodetachment spectroscopy, including photoelectron imaging methods.[12–16] If three of the values

appearing in Eq. (1.2) or (1.3) are known, the fourth can be calculated; if all four experimental values are known, the thermochemical cycle can be tested to confirm self-consistency. In the case of divanadium, V_2, for example, all four quantities in Eq. (1.2) have been independently measured,[17–21] and excellent agreement was obtained between the left and right sides of the equation (0.002 eV). In this example, the BDEs of V_2 and V_2^+ were measured by the observation of a sharp predissociation threshold in a highly congested vibronic spectrum, the same technique as employed in this work. This superb level of agreement in the case of V_2 confirms that when there is a sufficiently large density of states, the molecule finds a way to dissociate as soon as the ground separated atom limit is exceeded.

Because of the importance of bond dissociation energies and the challenge of calculating them accurately using *ab initio* or density functional theory (DFT) methods,[22] the development of computational methods for accurate BDE calculations remains an active research field. This is of particular importance in transition metal, lanthanide, and actinide systems, where electron correlation and relativistic effects combine to complicate matters severely.[23–31] A proposed goalpost for computational studies is to obtain the correct thermodynamic value to within 3 kcal/mol (0.13 eV) for transition metal species,[22] although in some cases a value off by only 1 kcal/mol (0.04 eV) is possible.[31] A fundamental problem is a lack of high quality experimental data to use as benchmarks. Much of the existing data is of relatively low precision; worse, for many species, no measurements of the BDE have been reported.[32] This is partially due to the challenging nature of studying gaseous transition metal species, which in equilibrium-based

methods require extremely high temperatures. In addition, many experiments do not directly observe dissociation, but calculate the bond dissociation energy from quantities measured in that experiment.[31] For example, Knudsen effusion mass spectrometry measures high temperature gas-phase chemical equilibrium,[33–35] and the bond energy is found by analysis via the second or third law of thermodynamics.[36] The analysis requires statistical thermodynamic assumptions about the molecules in equilibrium, and this can lead to significant errors. Another common method to obtain bond energies is through Eq. (1.2) or (1.3), leading to errors limited by the uncertainties of the quantities that are combined to obtain the BDE.

To remedy the lack of high-quality experimental data, we have been working to develop a broad database of d- and f-block metal bond dissociation energies. In the past, we have reported BDEs of diatomic transition metal molecules;[17–19,37–42] more recently, our focus has shifted to transition metals—main group diatomics.[36,43–47] The present study of the BDEs of FeSi, RuSi, OsSi, CoSi, RhSi, IrSi, NiSi, and PtSi adds to our previous work on the TiSi, ZrSi, HfSi, VSi, NbSi, and TaSi molecules.[46] Altogether, we have now measured the BDEs of 14 diatomic transition metal silicides. In addition to developing a broad set of benchmarks for calibration of computational methods, we also seek to understand the bonding patterns and chemical trends by investigating this series of chemically related species.

Transition metal-silicon bonding has long been of interest, mainly due to the use of these species in solid state devices, where doped silicon is widely employed. As noted in our previous paper on early transition metal silicides,[46] the main properties of interest include the unique semiconducting properties, high temperature stability, and corrosion resistance of the metal silicides. In addition, precise knowledge of the silicon-metal interaction is expected to become more important as the device size continues to shrink.[12] Additional interest arises from predictions of finding FeSi as a component in circumstellar dust,[48] and possibly as a small percent of the earth's core.[49] Computationally, the most interesting and challenging molecules studied here are the heaviest ones: OsSi, IrSi, and PtSi. In these species, the challenge of an open $5d$ subshell is combined with significant relativistic effects, including spin-orbit interaction.

All of these BDEs were measured by observing a sharp drop in the ion signal obtained using the resonant two-photon ionization (R2PI) method as the excitation laser is scanned to the blue. The sharp drop from a quasicontinuous absorption spectrum to the baseline corresponds to the predissociation threshold of the molecule. We argue that this occurs at the thermochemical bond dissociation energy, as in these species the large number of potential curves arising from the ground and low-lying separated atom limits ensures that when the bond energy is exceeded, the molecule is able to find a pathway to dissociate. This may occur by direct excitation into a state that correlates to ground state atoms, or by exciting into a bound state correlating to a higher separated atom limit that is coupled by nonadiabatic or spin-orbit interactions to states correlating to the ground separated atom limit. Essentially, once the excitation energy exceeds the dissociation energy, the molecule finds a way to fall apart on a ns to sub-ns time scale. Rigorously,

an observed predissociation threshold only provides an upper limit to the BDE, as a barrier to dissociation could cause the threshold to appear at a higher energy. In practice, because of the high density of states in these species, we believe that dissociation occurs promptly to the ground separated atom limit, and that the measured predissociation threshold provides a direct measurement of the bond dissociation energy.

Unlike the other metals studied here, which have D_g or F_g ground terms, palladium has a $4d^{10} 5s^0$, ^1S_g ground term. This leads to a much lower density of states at the Pd, ^1S_g + Si, ^3P_g ground separated atom limit than in the other MSi molecules. As a result, PdSi is unlikely to display a sharp predissociation threshold that can be interpreted as its thermochemical bond dissociation energy. For this reason, no attempt was made to measure the BDE of PdSi at this time.

II. EXPERIMENTAL METHODS

All data were collected using the same method reported in our recent bond energy studies and in the same instrument used for our previous group 4 and 5 transition metal silicide BDE measurements.[46] The molecule of interest is created by laser ablation of a rotating and translating metal sample disk (pure elements, except for a 1:1 VFe alloy used for FeSi and a 1:1 VOs alloy used for OsSi). The ablation laser pulse ejects metal atoms from the sample, forming a plasma of atoms, atomic ions, and electrons that is entrained in the carrier gas, a mixture of 0.13% silane in helium. Reactions readily occur in this hot environment, forming MSi molecules along with other species. The plasma is then carried through a channel (5 mm diameter, 1 cm long), which allows vibrational and electronic cooling of the nascent species via collisions with helium. The carrier gas and its contents then undergo supersonic expansion into vacuum (10^{-5} Torr) through a 5 mm diameter final orifice. The details of the chemical reactions occurring in the source are unknown, but a variety of atoms, diatomic species, and larger clusters are produced, depending on the vaporization laser power, carrier gas pressure, reactant gas concentration, and details of the nozzle geometry. Experimental conditions are adjusted to optimize the production of the MSi molecule of interest.

The supersonic expansion cools the MSi molecules and other species, which pass through a skimmer into a second chamber containing a resonant two-photon ionization (R2PI) ion source which produces ions in the extraction region of a Wiley-McLaren time-of-flight mass spectrometer (TOFMS).[50] The resulting ions are extracted into a time-of-flight mass spectrometer that is orthogonally oriented relative to the molecular beam path. In the present study, the molecules are electronically excited using a tunable optical parametric oscillator (OPO) laser, and then ionized after a short delay (20-80 ns) by an excimer laser (KrF mix; 248 nm, 5.00 eV). The laser intensities are reduced using filters so that the combination of both photons is needed for ionization. The ion signal due to multiphoton processes involving either laser alone is negligible.

As the ions are created in an electric field and share a common electrical potential, they are accelerated into the time-of-flight region and separate by mass before striking a

dual microchannel plate detector. Because multiple masses can be monitored independently, various species and isotopes are simultaneously recorded. The atomic transitions observed are compared to known values to calibrate the wavenumber axis.[1] Generally, calibration atomic signals are recorded concurrently and are easily identified, but sometimes additional atomic spectra are recorded for calibration purposes. In the present study, this was done for FeSi (Nb atomic spectra were used, as Fe is resonant with the KrF excimer wavelength, leading to an enormous and constant background signal at the mass of Fe^+), OsSi (where calibration was supplemented with V atomic transitions, in order to obtain a higher density of calibration wavelengths near the OsSi predissociation threshold), and NiSi (where signal from ^{64}Ni was used to supplement ^{58}Ni, as the ^{58}Ni signal was so intense that the microchannel plates were saturated, broadening the more intense features).

Final spectra are averages of at least three scans, with 30 shots averaged at each wavelength point during each scan. Once the atomic peaks are identified, the wavenumber axis of the averaged spectrum is shifted to align with the known atomic transition wavenumbers.[1] The residual error is a few wavenumbers at most and is included in the reported error limits. The other major source of error is subjectivity in assigning the threshold, which in ambiguous cases leads to larger reported error limits.[47] This was not a significant issue for the BDEs reported here.

III. RESULTS

A scan over the predissociation threshold of FeSi is displayed in Fig. 1. At energies below the predissociation threshold at 19 370 cm^{-1} (2.402 eV), a weak, continuous absorption spectrum is observed. This is due to the high density of electronic states in the molecule. Superimposed on this weak, continuous absorption is a much stronger vibronic progression.
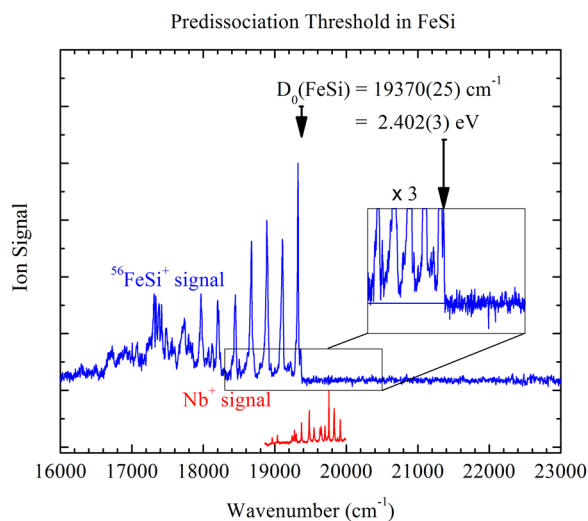

FIG. 1. R2PI spectrum of FeSi, showing predissociation threshold at 19 370(25) cm^{-1}. Strong vibronic features are observed on top of a weak continuous absorption below the threshold. The vertically expanded inset shows that the weak absorption lies measurably above the extrapolated baseline until the sharp drop to baseline is reached, allowing the BDE to be determined precisely. The reported uncertainty range is indicated for this and all other species by the black bar on the top of the arrow. The Nb atomic spectrum displayed in the lower trace was used for calibration.
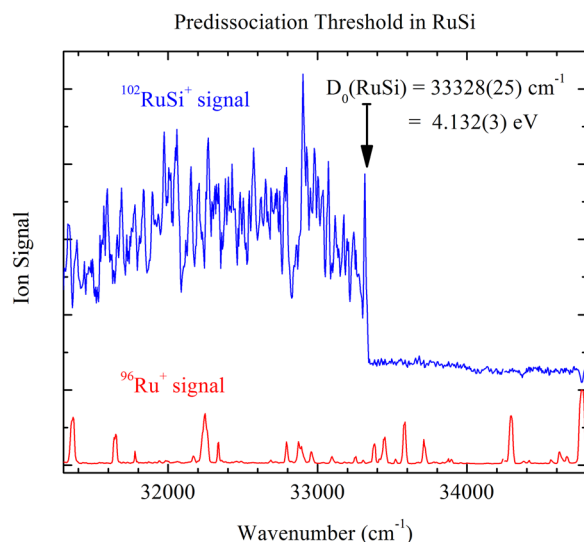

FIG. 2. R2PI spectrum of RuSi (upper trace) showing predissociation threshold at 33 328(25) cm^{-1}. The Ru atomic spectrum displayed in the lower trace was used for calibration.

This is presumably due to an excited electronic state that correlates to an excited separated atom limit whose potential energy curve dips below the ground separated atom limit. These vibrational features are probably more intense than the underlying quasi-continuum due to more favorable Frank-Condon overlap with the ground state, possibly combined with a more favorable transition dipole moment. At higher energies than the identified threshold, a flat baseline is observed, with no significant $FeSi^+$ ion signal. As discussed in Sec. II, atomic Nb was used to calibrate the spectrum in separate scans employing a niobium sample.

The dissociation threshold of FeSi clearly falls before the next expected member of the vibronic progression, which is expected near 19 520 cm^{-1}. However, an expanded view of the threshold region shows that even between the members of the vibronic progression, the ion signal remains above the baseline
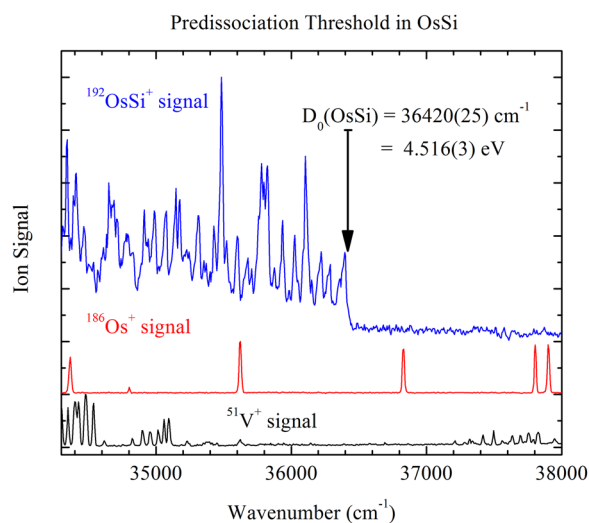

FIG. 3. R2PI spectrum of OsSi (upper trace), showing predissociation threshold at 36 420(25) cm^{-1}. The lower traces show the atomic spectra of Os (middle trace), and V (lower trace). Both atomic spectra were used for calibration.

Predissociation Threshold in CoSi

$CoSi^+$ signal

$D_0(CoSi) = 23085(25)$ cm^{-1}
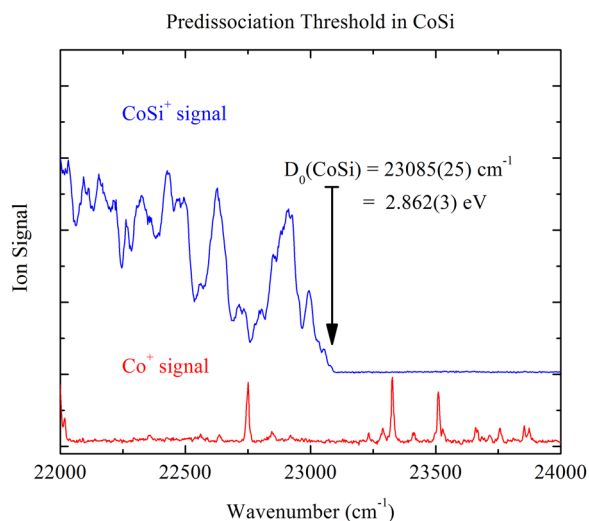$= 2.862(3)$ eV

Co^+ signal

FIG. 4. R2PI spectrum of CoSi (upper trace), showing predissociation threshold at 23 085(25) cm^{-1}. The Co atomic spectrum (lower trace) was used for calibration.

Predissociation Threshold in IrSi

$^{193}IrSi^+$ signal

$D_0(IrSi) = 39938(25)$ cm^{-1}
$= 4.952(3)$ eV

$^{193}Ir^+$ signal

FIG. 6. R2PI spectrum of IrSi (upper trace), showing predissociation threshold at 39 938(25) cm^{-1}. The Ir atomic spectrum displayed in the lower trace was used for calibration.

due to the underlying quasi-continuous absorption. This weak continuous absorption drops promptly to the baseline slightly above the last observed vibronic band, at 19 370 cm^{-1}. On this basis, we assign the BDE of FeSi to be 19 370(25) cm^{-1}, or 2.402(3) eV.

Figures 2–8 show spectra for scans over the predissociation thresholds of RuSi, OsSi, CoSi, RhSi, IrSi, NiSi, and PtSi, respectively, along with the atomic spectra that were used for calibration. All of these spectra, with the exception of PtSi, display a sharp drop to a flat baseline that allows the predissociation threshold to be identified to a precision of ±25 cm^{-1} (0.003 eV). In these cases, the sharp predissociation threshold is assigned as the thermochemical bond dissociation energy of the molecule, providing BDE values as indicated on Figs. 1–7. In the case of PtSi, a few much weaker features persist for about 100 cm^{-1} above the apparent predissociation threshold, introducing some ambiguity about the precise location

of the threshold. Accordingly, we adopt a more conservative error limit for PtSi, increasing our error limits to ±75 cm^{-1} (0.009 eV). A possible explanation of these weak features may be found in the correlation between molecular states and the separated atom limits, described below.

In these predissociation threshold experiments, it is important to consider whether there may be symmetry-based restrictions that could prevent dissociation at the ground separated atom limit.[1] The supersonic expansion cools molecules produced in our source, probably to a few tens of kelvin,[51] and therefore the population resides almost exclusively in the ground vibronic level of the molecule. In order for the electronically excited molecule to promptly dissociate to the ground separated atom limit when the dissociation energy is exceeded, the total angular momentum about the axis, Ω, must be conserved unless rotationally-induced nonadiabatic processes are

Predissociation Threshold in RhSi

$RhSi^+$ signal

$D_0(RhSi) = 33629(25)$ cm^{-1}
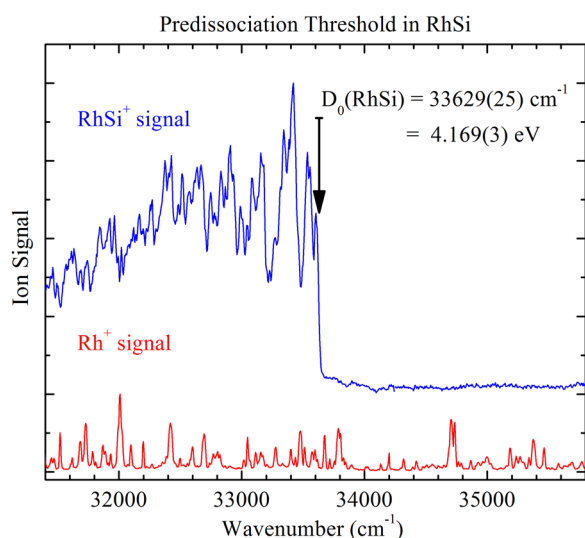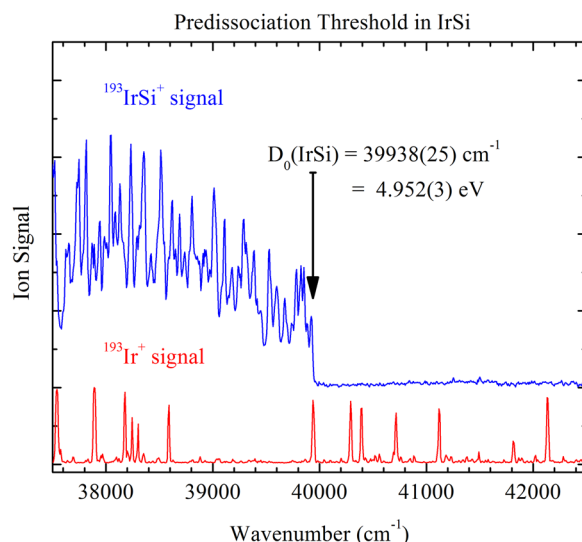$= 4.169(3)$ eV

Rh^+ signal

FIG. 5. R2PI spectrum of RhSi (upper trace), showing predissociation threshold at 33 629(25) cm^{-1}. The Rh spectrum displayed in the lower trace was used for calibration.

Predissociation Threshold in NiSi

$^{58}Ni^{28}Si^+$ signal

$D_0(NiSi) = 26809(25)$ cm^{-1}
$= 3.324(3)$ eV
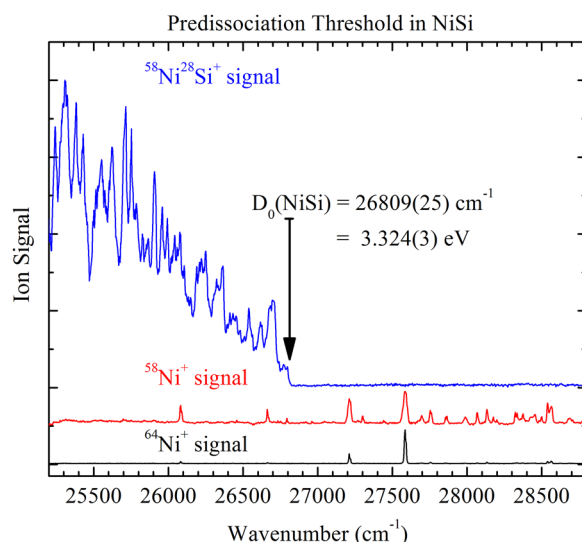
$^{58}Ni^+$ signal

$^{64}Ni^+$ signal

FIG. 7. R2PI spectrum of NiSi (upper trace), showing predissociation threshold at 26 809(25) cm^{-1}. The atomic spectra of ^{58}Ni (middle trace) and ^{64}Ni (lower trace) were used for calibration.
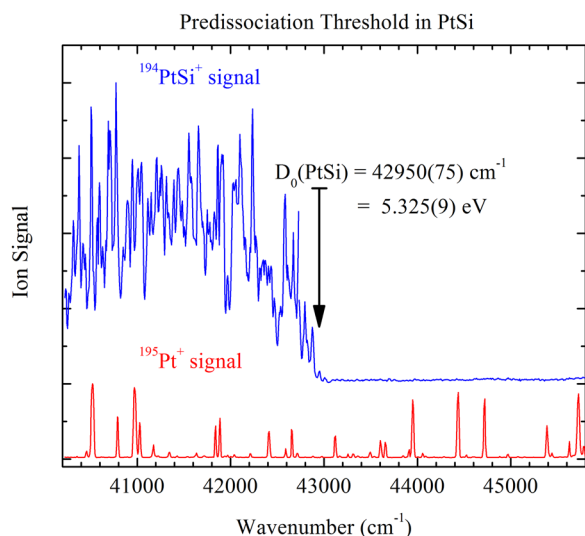
FIG. 8. R2PI spectrum of PtSi (upper trace), showing predissociation threshold at 42 950(75) cm^{-1}. The Pt atomic spectrum displayed in the lower trace was used for calibration.

considered. Upon photoexcitation, the Ω'' level arising from the ground state can keep the same value or change by up to one unit ($\Delta\Omega = 0, \pm 1$). Thus, the question is: Do the Ω states arising from the ground separated atom limit contain a match with the Ω' states that can be reached via transitions from the molecular ground state? As shown in Table I, with the exception of PtSi, this condition is met for all of the molecules considered in this report.

For PtSi, the ground state is $^1\Sigma^+$,[52,53] which possesses only $\Omega'' = 0^+$. States that are optically accessible have $\Omega' = 0^+$ or 1. The ground separated atom limit of Pt, $^3D_{3g}$ + Si $^3P_{0g}$ generates Ω states with $\Omega = 3, 2, 1,$ or 0^-,[54,55] so the excited states with $\Omega' = 1$ can dissociate to ground state atoms while preserving Ω, but those with $\Omega' = 0^+$ cannot. If the value of Ω' is to be preserved in the dissociation process, states with $\Omega' = 0^+$ can only dissociate at the excited Pt, $^3D_{3g}$ + Si $^3P_{1g}$ limit, 77 cm^{-1} above the ground separated atom asymptote. This limit generates an $\Omega = 0^+$ state that allows dissociation to preserve the Ω value.

While these considerations are valid for the nonrotating molecule, heterogeneous perturbations due to the **S**- and **L**-uncoupling operators allow the $\Omega' = 0^+$ states (which have only e parity levels) to couple to the e parity levels of an $\Omega = 1$ state.[56] Thus, all of the optically accessible states in PtSi, with the exception of the $\Omega' = 0^+$, J = 0 levels, can dissociate at the ground separated atom limit, although the heterogeneous perturbation that makes this possible will be weak for the smaller values of J. As a result, for PtSi one might expect a double threshold, with the majority of the excited states dissociated promptly at the ground separated atom limit and a smaller fraction of the excited molecules failing to dissociate until the Pt, $^3D_{3g}$ + Si $^3P_{1g}$ limit is reached, 77 cm^{-1} above the ground separated atom limit. The analogous situation has been clearly observed in the cases of V_2 and Zr_2,[17,18,39] and less definitely in the case of WSi.[45] It is possible that the weakest features observed just before the baseline goes flat in Fig. 8 correspond to excited states with $\Omega' = 0^+$ that can only dissociate to ground state atoms via rotationally-induced nonadiabatic perturbations. The selected error limit of ± 75 cm^{-1} is sufficient to cover this ambiguity, giving a final result of D_0(PtSi) = 5.325(9) eV.

IV. DISCUSSION

A. FeSi, RuSi, and OsSi

Previous studies of FeSi, RuSi and OsSi are summarized in Table II. The only previous bond energy measurements come from Knudsen effusion studies of FeSi and RuSi. The previous value for D_0(RuSi), combined with its reported error limit, encompasses our result. The Knudsen effusion measurement for FeSi, however, is about 0.6 eV higher than our value, a serious discrepancy. Most of the computed BDEs for the FeSi, RuSi, and OsSi molecules are significantly smaller than our values;[57,58] the exception is the recently reported multi-state N-electron valence state second-order perturbation theory (MS-NEVPT2) calculation on OsSi, which exceeds our measured BDE by 1.25 eV.[59] This large computational error illustrates the need for both good measurements and improved computational methods.

TABLE I. Correlation of molecular states to separated atom states.

Molecule	Ground term	Reference for molecular term	Molecular ground Ω'' value	Optically accessible Ω' values	Ground separated atom limit[a]	Separated atom limit Ω values[b]
FeSi[c]	$^3\Sigma^-$	58	0^+	0^+, 1	$^5D_{4g}$ + $^3P_{0g}$	0^+, 1, 2, 3, 4
	$^3\Delta$	57	3	2, 3, 4		
RuSi	$^3\Delta$	60	3	2, 3, 4	$^5F_{5g}$ + $^3P_{0g}$	0^-, 1, 2, 3, 4, 5
OsSi	$^3\Sigma^-$	51	0^+	0^+, 1	$^5D_{4g}$ + $^3P_{0g}$	0^+, 1, 2, 3, 4
CoSi[c]	$^2\Sigma^+$	34, assumed	1/2	1/2, 3/2	$^4F_{9/2g}$ + $^3P_{0g}$	1/2, 3/2, 5/2, 7/2, 9/2
	$^2\Delta$	58	5/2	3/2, 5/2, 7/2		
RhSi	$^2\Sigma^+$	61	1/2	1/2, 3/2	$^4F_{9/2g}$ + $^3P_{0g}$	1/2, 3/2, 5/2, 7/2, 9/2
IrSi	$^2\Delta$	63	5/2	3/2, 5/2, 7/2	$^4F_{9/2g}$ + $^3P_{0g}$	1/2, 3/2, 5/2, 7/2, 9/2
NiSi	$^1\Sigma^+$	64	0^+	0^+, 1	$^3F_{4g}$ + $^3P_{0g}$	0^+, 1, 2, 3, 4
PtSi	$^1\Sigma^+$	52 and 53	0^+	0^+, 1	$^3D_{3g}$ + $^3P_{0g}$	0^-, 1, 2, 3

[a]From Ref. 1.
[b]Derived using the Wigner-Witmer correlation rules found in Refs. 54 and 55.
[c]For all molecules except FeSi and CoSi, the ground term has been experimentally determined. For these molecules, the possible ground terms have been computationally derived.

TABLE II. Previous studies of FeSi, RuSi, and OsSi.[a]

Molecule	Ground term	D_0 (eV)	Method	Authors	Year	References
FeSi		**2.402(3)**	Threshold		2018	This work
	$^1\Sigma$ (assumed)	**3.04(26)**	Knudsen effusion	Auwera-Mahieu et al.	1969	34
	$^3\Delta$	1.98	MRSDCI + Q	Sekiya et al.	2003	57
	$^3\Sigma^-$	2.09	DFT calculation	Wu and Su	2006	58
RuSi		**4.132(3)**	Threshold		2018	This work
	$^1\Sigma$ (assumed)	**4.08(22)**	Knudsen effusion	Auwera-Mahieu et al.	1969	35
	$^3\Delta$	3.74	DFT calculation	Wu and Su	2006	58
	$^3\Delta_3$		R2PI spectroscopy	Lindholm and Morse	2007	60
OsSi		**4.516(3)**	Threshold		2018	This work
		4.14	DFT calculation	Wu and Su	2006	58
	$^3\Sigma^-_{0^+}$		R2PI spectroscopy	Johnson and Morse	2015	51
	$^3\Sigma^-_{0^+}$	5.76	MS-NEVPT2 calculation	Suo et al.	2018	59

[a]Quantities obtained from experimental measurements are given in **bold**; computed quantities are given in plain text.

The qualitative molecular orbital structure of all of the molecules investigated here may be understood by considering the combinations of the valence orbitals on the metal [nd and (n + 1)s] and on Si (3s and 3p). These combine to form four σ orbitals, two pairs of π orbitals, and one pair of δ orbitals. The resulting orbitals, displayed in Fig. 9 for NiSi, are qualitatively given as:

- 1σ, a silicon 3s-like orbital making a mostly nonbonding contribution.
- 2σ, mainly consisting of metal ndσ and Si 3pσ bonding overlap.
- 1π, a bonding orbital composed of metal ndπ and Si 3pπ character.
- 1δ, a pair of nonbonding orbitals which are almost purely metal ndδ orbitals.
- 3σ, a mostly nonbonding orbital composed mainly of the metal (n + 1)s orbital, with some bonding character to the Si 3pσ orbital.
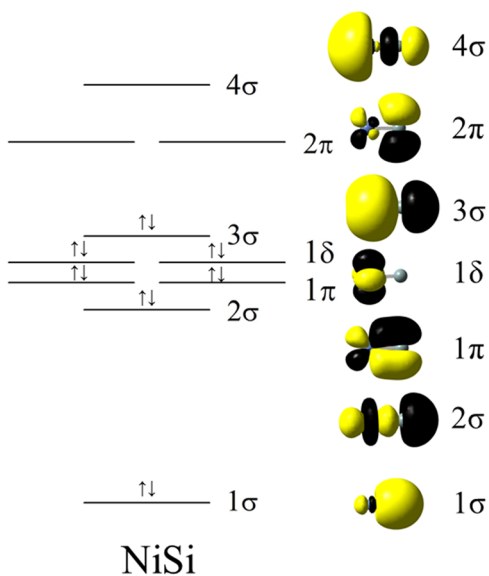
- The 2π and 4σ antibonding orbitals, matched with the 1π and 2σ orbitals, respectively.

Using this notation allows multiple species to be compared conveniently even though the order and energy spacing of these orbitals changes between molecules.[51] In all of the molecules investigated here, the 1σ, 2σ, and 1π orbitals are filled in the ground states. For the Fe series, an additional four electrons must be accounted for. For FeSi, Sekiya et al., using the MRSDCI+Q method, obtained a $1\delta^3 \, 3\sigma^1$, $^3\Delta$ ground term,[57] while Wu and Su obtained a $1\delta^2 \, 3\sigma^2$, $^3\Sigma^-$ ground term using B3LYP/LANL2DZ density functional theory.[58] Unfortunately, the ground term of FeSi has not yet been experimentally determined. For RuSi, rotationally resolved spectra confirm that the ground term is $1\delta^3 \, 3\sigma^1$, $^3\Delta_3$,[60] as obtained in the B3LYP/LANL2DZ calculations of Wu and Su.[58] For OsSi, relativistic stabilization of the 6s orbital causes a stabilization of the 3σ orbital, leading to an OsSi ground term of $1\delta^2 \, 3\sigma^2$, $^3\Sigma^-$.[51] This is also in agreement with the B3LYP/LANL2DZ calculations of Wu and Su and the high-level MS-NEVPT2 calculation of Suo et al.[58,59]

B. CoSi, RhSi, and IrSi

Table III presents a summary of previous studies on CoSi, RhSi, and IrSi. In these cases, the Knudsen effusion results are all within the experimental error of our values. For IrSi, the computed BDE of Wu and Su, 4.95 eV, is in superb agreement with our value of 4.952(3) eV, but for the other two molecules their results are about 0.5 eV too low.[58] Both RhSi and IrSi have been spectroscopically investigated, and the ground states are known to be $1\delta^4 \, 3\sigma^1$, $^2\Sigma^+$ and $1\delta^3 \, 3\sigma^2$, $^2\Delta_{5/2}$, respectively.[61–63] This is in agreement with the computational results.[58] The ground term of CoSi has been computed to be $1\delta^3 \, 3\sigma^2$, $^2\Delta_{5/2}$,[58] but this is not yet experimentally known. As in the FeSi, RuSi, OsSi series, the difference in ground state configuration between RuSi and OsSi is attributed to relativistic stabilization of the 3σ nonbonding orbital.[63]

FIG. 9. Molecular orbital diagram for NiSi.

TABLE III. Previous studies of CoSi, RhSi, and IrSi.[a]

Molecule	Ground term	D_0 (eV)	Method	Authors	Year	References
CoSi		**2.862(3)**	Threshold		2018	This work
	$^2\Sigma$ (assumed)	**2.81(18)**	Knudsen effusion	Auwera-Mahieu et al.	1969	34
	$^2\Delta$	2.36	DFT calculation	Wu and Su	2006	58
RhSi		**4.169(3)**	Threshold		2018	This work
	$^2\Sigma$ (assumed)	**4.05(19)**	Knudsen effusion	Auwera-Mahieu et al.	1969	35
	$^2\Sigma^+$	3.59	DFT calculation	Wu and Su	2006	58
	$^2\mathbf{\Sigma^+}$		LIF, DF spectroscopy	Adam et al.	2009	61
IrSi		**4.952(3)**	Threshold		2018	This work
	$^2\Sigma$ (assumed)	**4.76(22)**	Knudsen effusion	Auwera-Mahieu et al.	1969	35
	$^2\Delta$	4.95	DFT calculation	Wu and Su	2006	58
	$^2\mathbf{\Delta_{5/2}}$		R2PI spectroscopy	Garcia et al.	2013	63
	$^2\mathbf{\Delta_{5/2}}$		LIF spectroscopy	Le et al.	2013	62

[a]Quantities obtained from experimental measurements are given in **bold**; computed quantities are given in plain text.

C. NiSi and PtSi

Nickel and platinum silicides have been studied more extensively than the other species in this report. Table IV summarizes previous work. The three previous BDE measurements, one for PtSi and two for NiSi,[34,35,64] are in good agreement with our values, although much less precise. For NiSi, the first of these values is from a Knudsen effusion study,[34] while the second is an extrapolation of the vibrational energy levels to the dissociation limit,[64] using the equation

$$D_e = \frac{\omega_e^2}{4\omega_e x_e}. \qquad (4.1)$$

This extrapolation assumes that higher order anharmonicities may be neglected and that the vibrational levels may be modeled as

$$G(v) = \omega_e\left(v + \frac{1}{2}\right) - \omega_e x_e\left(v + \frac{1}{2}\right)^2 \qquad (4.2)$$

all the way to dissociation. The resulting D_e value is then converted to D_0 in Table IV. Vibrational extrapolation using Eq. (4.1) is often unreliable, because higher order anharmonicities or perturbations of the observed vibrational levels can throw off the predicted dissociation energies, sometimes by as much as 1 eV. The method can work when there are no perturbations of the observed vibrational levels, and a large number of vibrational levels are measured, as was the case for NiSi.[64] In previous work, we have found that this method of extrapolation gave very poor results for FeC, FeS, and NiS, but was much better for NiC.[44] The excellent agreement for NiSi and good agreement for NiC suggests that higher order anharmonicities are small for these species, and that the ground states are relatively free of perturbations.[44] The ground terms of NiC, NiSi, PtC, and PtSi are all closed shell $1\delta^4 3\sigma^2$, $^1\Sigma^+$ terms, in which the bonding and nonbonding orbitals are fully occupied. Excited states must place an electron in an antibonding orbital, leading to a significant gap between

TABLE IV. Previous studies of NiSi and PtSi.[a]

Molecule	Ground term	D_0 (eV)	Method	Authors	Year	References
NiSi		**3.324(3)**	Threshold		2018	This work
	$^1\Sigma$ (assumed)	**3.26(18)**	Knudsen effusion	Auwera-Mahieu et al.	1969	34
	$^1\Sigma^+$		HF-CI calculation	Shim and Gingerich	1988	67
	$^1\Sigma^+$	1.88	MRDCI calculation	Haberlandt	1989	68
	$^1\Sigma^+$	2.35	CASSCF calculation	Shim and Gingerich	1990	69
	$^1\mathbf{\Sigma^+}$	**3.31(3)**	R2PI/Morse potential extrapolation	Lindhom et al.	2002	64
	$^1\Sigma^+$	2.30	DFT calculation	Wu and Su	2006	58
	$^1\Sigma^+$	3.27	CCSD(2)$_T$	Schoendorff et al.	2015	66
PtSi		**5.325(9)**	Threshold		2018	This work
	$^1\Sigma$ (assumed)	**5.15(19)**	Knudsen effusion	Auwera-Mahieu et al.	1969	35
	$^1\mathbf{\Sigma^+}$		Cavity ringdown	Paul et al.	1995	52
	$^1\mathbf{\Sigma^+}$		R2PI spectroscopy	Shao et al.	1999	53
	$^1\Sigma^+$	5.16	CASPT2	Barysz and Pyykkö	2002	70
	$^1\mathbf{\Sigma^+}$		Pure rotational spectroscopy	Cooke et al.	2004	77
	$^1\Sigma^+$	5.00	DFT calculation	Wu and Su	2006	58

[a]Quantities obtained from experimental measurements are given in **bold**; computed quantities are given in plain text.

the ground and first excited states. We surmise that the rel-atively large gap between the ground and first excited states in these species accounts for the accuracy of the vibrational extrapolation.[65,66]

Older hypotheses and computational studies of both NiSi and PtSi differed from the bonding description discussed above, with the metal s orbital (4s or 6s) interacting with the silicon Si $3p\sigma$ orbital as the main component and with minor bonding between the metal $nd\pi$ and silicon $3p\pi$.[53,67–69] More recent descriptions have slightly shifted; Schoendorff *et al.* found that the nickel $3d\sigma$ orbital hybridizes with the metal 4s, forming one orbital that is nonbonding and one that is suitable for σ bonding interactions with the silicon $3p\sigma$ orbital; they also find that the silicon $3p\pi$ orbitals form a pair of π bonds with the nickel $3d\pi$ orbitals.[66] For PtSi, Barysz and Pyykkö likewise calculated that the platinum 6s and $5d\sigma$ orbitals con-tribute to the σ bond, while the silicon $3p\pi$ and $5d\pi$ orbitals form a pair of bonds to give a net bond order of three.[70] These more recent descriptions are qualitatively similar to what is described above, with the metal $nd\delta$ and silicon $3s\sigma$ orbitals being nonbonding, while one σ and two π bonds are formed between the metal nd and silicon $3p$ orbitals, leading to a triple bond.

TABLE V. Derived enthalpies of formation at 0 K of the MSi molecules.[a]

		Si
$\Delta H^\circ_{f,0K}$ (kJ mol^{-1})		**445.7(8.0)**
Fe	**413.1(1.3)**	627.0(8.1)
Ru	**652.7(6.3)**	699.7(10.2)
Os	**789.1(6.3)**	799.0(10.2)
Co	**425.1(2.1)**	594.6(8.3)
Rh	**555.2(2.1)**	598.6(8.3)
Ir	**668.6(6.3)**	636.5(10.2)
Ni	**428.1(8.4)**	553.0(11.6)
Pt	**564.8(2.1)**	496.7(8.3)

[a]The bolded entries are the atomic enthalpies of formation used in the calculations. These values are taken from Ref. 78 for Fe, Co, Ni, and Si, and from Ref. 79 for Ru, Os, Rh, Ir, and Pt.

D. Derived quantities

Using reference values of enthalpies of formation of the gaseous metal and silicon atoms, the measured BDEs of the MSi molecules may be employed in Eq. (1.1) to obtain enthalpies of formation of the gaseous MSi molecules. These are provided in Table V.

TABLE VI. Ground state configurations, terms, and BDEs (eV) of Transition Metal Silicides.[a]

ScSi[b]	TiSi[c]	VSi[d]	CrSi[e]	MnSi[e]	FeSi[f]	CoSi[g]	NiSi[h]	CuSi[i]
$[1\pi^2 3\sigma^1]$	$[1\pi^2 1\delta^1 3\sigma^1]$		$[1\pi^3 1\delta^2 3\sigma^1]$	$[1\delta^2 3\sigma^1]$		$[1\delta^3 3\sigma^2]$	$1\delta^4 3\sigma^2$	$1\delta^4 3\sigma^2 2\pi^1$
$[^4\Sigma^-_{1/2}]$	$[^5\Delta]$		$[^5\Pi]$	$[^4\Sigma^-_{1/2}]$		$[^2\Delta]$	$^1\Sigma^+$	$^2\Pi_{1/2}$
2.31(15)	2.201(3)	2.234(3)	[1.54]	[1.76]	2.402(3)	2.862(3)	3.324(3)	2.26(6)
YSi[j]	ZrSi[k]	NbSi[l]	MoSi[m]	TcSi[e]	RuSi[n]	RhSi[o]	PdSi[p]	AgSi[q]
$[1\pi^2 3\sigma^1]$		$1\pi^4 1\delta^1$		$[1\delta^2 3\sigma^1]$	$1\delta^3 3\sigma^1$	$1\delta^4 3\sigma^1$	$1\delta^4 3\sigma^2$	$1\delta^4 3\sigma^2 2\pi^1$
$[^4\Sigma^-_{1/2}]$		$^2\Delta_{3/2}$		$[^4\Sigma^-_{1/2}]$	$^3\Delta_3$	$^2\Sigma^+$	$^1\Sigma^+$	$^2\Pi_{1/2}$
2.63(18)	2.950(3)	3.080(3)	[2.06]	[3.69]	4.132(3)	4.169(3)	2.66(12)	1.80(11)
LaSi[e]	HfSi[r]	TaSi[r]	WSi[s]	ReSi[e]	OsSi[t]	IrSi[u]	PtSi[v]	AuSi[w]
$[2\sigma^1 1\pi^4]$	$[1\pi^3 3\sigma^1]$	$[1\pi^3 1\delta^1 3\sigma^1]$		$[1\delta^2 3\sigma^1]$	$1\delta^2 3\sigma^2$	$1\delta^3 3\sigma^2$	$1\delta^4 3\sigma^2$	$1\delta^4 3\sigma^2 2\pi^1$
$[^2\Sigma^+]$	$[^3\Pi]$	$[^4\Phi]$		$[^4\Sigma^-_{1/2}]$	$^3\Sigma^-(0^+)$	$^2\Delta_{5/2}$	$^1\Sigma^+$	$^2\Pi_{1/2}$
[2.46]	2.871(3)	2.999(3)	3.103(10)	[3.12]	4.516(3)	4.952(3)	5.325(9)	3.12(6)

[a]Computational results are given in square brackets.
[b]Configuration and term from Ref. 58. BDE from Ref. 80.
[c]Configuration and term from Refs. 58 and 81. BDE from Ref. 46.
[d]Configuration and term poorly known, calculated to be $1\pi^2 1\delta^2 3\sigma^1$, $^6\Sigma^+$ or $1\pi^3 1\delta^1 3\sigma^1$, $^4\Pi/\Phi$ in Refs. 46 and 58; thought to be $1\pi^4 1\delta^1$, $^2\Delta_{3/2}$ from ESR studies in Ref. 82. BDE from Ref. 46.
[e]Configuration, term, and BDE calculated in Ref. 58.
[f]The ground configuration and term have been calculated to be $1\pi^4 1\delta^2 3\sigma^2$, $^3\Sigma^-$ in Ref. 58; $1\pi^4 1\delta^3 3\sigma^1$, $^3\Delta$ in Ref. 57. BDE from this work.
[g]Configuration and term from Ref. 58. BDE from this work.
[h]Configuration and term from Ref. 64. BDE from this work.
[i]Configuration and term from Ref. 83. BDE from 84.
[j]Configuration and term from Ref. 58. BDE from Ref. 85.
[k]Configuration and term poorly known, calculated to be $1\pi^2 1\delta^1 3\sigma^1$, $^5\Delta$ in Refs. 58 and 46, and either $1\pi^2 1\delta^1 3\sigma^1$, $^5\Delta$; a triplet state of undefined symmetry; or $1\pi^4$, $^1\Sigma^+$ in Ref. 12. BDE from Ref. 46.
[l]Configuration and term poorly known, calculated to be $1\pi^3 1\delta^1 3\sigma^1$, $^4\Pi/\Phi$ in Refs. 46 and 58 with $1\pi^2 1\delta^2 3\sigma^1$, $^6\Sigma^+$ lying within 0.04 eV. These are calculated to be very close in energy in Ref. 12 also. Matrix isolation ESR studies suggest a $1\pi^4 1\delta^1$, $^2\Delta$ ground configuration and term in Ref. 82. BDE from Ref. 46.
[m]Configuration and term calculated to be either $1\pi^3 1\delta^2 3\sigma^1$, $^5\Pi$ or $1\pi^4 1\delta^1 3\sigma^1$, $^3\Delta$ in Refs. 58 and 12, with a small separation between them. BDE from the computation of Ref. 58.
[n]Configuration and term from Ref. 60. BDE from this work.
[o]Configuration and term from Ref. 61. BDE from this work.
[p]Configuration and term from Ref. 76. BDE from Ref. 86.
[q]Configuration and term from Ref. 87. BDE from Ref. 84.
[r]Configuration and term from Ref. 58. BDE from Ref. 46.
[s]Configuration and term are calculated to be $1\pi^3 1\delta^2 3\sigma^1$, $^5\Pi$ in Ref. 58 and either $1\pi^3 1\delta^2 3\sigma^1$, $^5\Pi$ or $2\sigma^1 1\pi^4 1\delta^2 3\sigma^1$, $^5\Sigma^-$ in Ref. 12. In Ref. 45, a $1\pi^4 1\delta^1 3\sigma^1$, $^3\Delta$ ground state is obtained. BDE is from Ref. 45.
[t]Configuration and term from Ref. 51. BDE from this work.
[u]Configuration and term from Ref. 63. BDE from this work.
[v]Configuration and term from Refs. 52 and 53. BDE from this work.
[w]Configuration and term from Refs. 58 and 88. BDE from Ref. 89.

The bond dissociation energies, $D_0(M^+–Si)$, have been measured by guided ion beam mass spectrometry (GIBMS) for the complete series of 3d transition metals, as well as for Y, La, and Lu.[71–74] Employing these values in combination with the thermochemical cycle of Eq. (1.2), the precisely known atomic ionization energies (Ref. 1), and our values of $D_0(MSi)$ allows ionization energies of the metal silicides to be determined as IE(FeSi) = 7.43(9) eV, IE(CoSi) = 7.49(7) eV, and IE(NiSi) = 7.62(7) eV. Our spectroscopic results also place limits on the ionization energy of these species, however, because the combination of one tunable photon that leads to an observable transition and one KrF excimer photon (5.00 eV) must be sufficient to ionize the molecule. In the case of CoSi and NiSi, we have not scanned far enough to the red to see the ion signal drop to zero; the ion signal is still observed at the red limits of the scanned region, 21 741 cm^{-1} and 25 055 cm^{-1} for CoSi and NiSi, respectively. Correcting for the electric field in the ion source (which induces a shift in the ionization potential of approximately −0.01 eV),[75] upper limits of IE(CoSi) < 7.70 eV and IE(NiSi) < 8.11 eV may be deduced. These are consistent with the values derived from the GIBMS experiments and the thermochemical cycle.

In the case of FeSi, however, Fig. 1 shows that a drop in ion signal to the baseline is observed near 16 600 cm^{-1} and a clearly distinguishable transition is observed at 17 306 cm^{-1}. The combination of these energies with the energy of the KrF ionization photon (5.00 eV) would imply that IE(FeSi) $\lesssim$ 7.07 eV or IE(FeSi) $\lesssim$ 7.16 eV, respectively. We adopt the more conservative result, IE(FeSi) $\lesssim$ 7.16 eV. Even so, this value remains inconsistent with the result obtained by combining our value of $D_0(FeSi)$, the accurately known IE(Fe), and the GIBMS value of $D_0(Fe^+–Si)$, which give IE(FeSi) = 7.43(9) eV. The 0.27 ± 0.09 eV discrepancy between these two values could be explained if the 17 306 cm^{-1} feature arose from vibrationally or electronically excited molecules, but this is not expected for a jet-cooled molecule with a low vibrational frequency, like FeSi. Alternatively, the discrepancy could be explained if our value of $D_0(FeSi)$ were too high, as could occur if there were a barrier to dissociation at the ground separated atom limit. A final possibility is that the GIBMS value of $D_0(Fe^+–Si)$ is too low. Further work will be required to understand the cause of this discrepancy.

For the remaining molecules, our results may be combined with atomic ionization energies to obtain the sum of the molecular ionization energy and the BDE of the cation, but these quantities cannot separately be determined from our currently available data.

E. Periodic trends

The bond energy trends for the MSi molecules as one moves across the transition metal series are summarized in Table VI and displayed in Fig. 10. Values obtained by the observation of a predissociation threshold, either in this or our previous studies,[45,46] are indicated by filled circles; values from other investigations are indicated by open squares. To our knowledge, no experimental data exist for the CrSi, MnSi, MoSi, TcSi, or ReSi molecules. Work is currently in progress in this group to obtain predissociation-based values of the BDEs of ScSi, YSi, and LaSi.
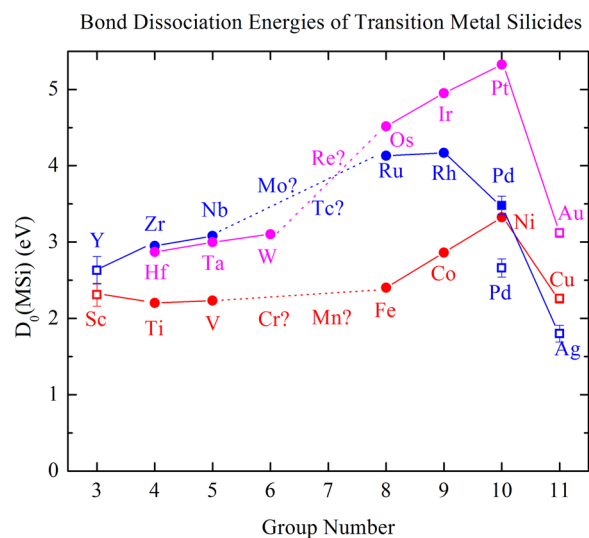

FIG. 10. Periodic trends in transition metal silicide bond dissociation energies. Solid circles represent predissociation-based measurements; open squares are values from Knudsen effusion mass spectrometry. For PdSi, the adiabatic or intrinsic bond dissociation energy is given by the filled blue square. The 3d series is given in red, the 4d series in blue, and the 5d series in magenta. Values for ScSi, CuSi, YSi, PdSi, AgSi, and AuSi are from the references cited in Table VI. Predissociation-based values are from this work and Refs. 45 and 46.

The most striking observation is that the BDEs of the 3d series of transition metal silicides are substantially smaller than the BDEs of the 4d and 5d series. This fact results from the small size of the 3d orbitals, which makes them less readily accessible for chemical bonding than the 4d and 5d orbitals in the heavier transition metals. Similarly, weaker BDEs are also found for the titanium and vanadium carbides and selenides, as compared to the carbides and selenides of the heavier 4d and 5d congeners.[43,47]

It is also noteworthy that the bond dissociation energies of the late transition metal silicides are significantly larger than those of the early transition metal silicides. The trend of increasing bond energies in the late transition metal silicides is particularly obvious in the FeSi, CoSi, NiSi and OsSi, IrSi, PtSi series. This is puzzling because all of these species are triply bonded, with one sigma and two pi bonds, differing only in the number and placement of electrons in the nominally nonbonding 1δ or 3σ orbitals. A similar pattern is found in the diatomic MC molecules, where possible causes have been discussed.[47] The abrupt bond energy drop in moving from RhSi to PdSi is partially due to the fact that the $^1\Sigma^+$ ground state of PdSi correlates to the Pd $4d^9 5s^1$, $^3D_{3g}$ + Si $3p^2$, $^3P_{1g}$ excited separated atom limit at 6641.26 cm^{-1} (0.823 eV).[1,55,76] Thus, the adiabatic or intrinsic bond dissociation energy of PdSi (indicated by the filled blue square) is 0.823 eV greater than the BDE measured in Knudsen effusion mass spectrometry (the open blue square). Even including this correction, a significant drop remains in BDE in going from RhSi to PdSi. This probably reflects the drop in the 4d orbital energies that occurs in the late 4d metals, where these orbitals are quickly becoming more core-like than in the 3d or 5d series. This trend continues as we move to AgSi, for which the BDE is even smaller than that of CuSi. The abrupt drop in BDE observed for CuSi, AgSi, and AuSi occurs because in these species,

the antibonding 2π orbital is singly occupied for the first time.

V. CONCLUSION

In this study, the observation of an abrupt onset of predissociation in a highly congested electronic spectrum has been used to measure the bond dissociation energies of the group 8, 9, and 10 diatomic transition metal silicides, MSi. The measured predissociation thresholds provide a rigorous upper bound on the bond dissociation energies of the molecules under study. Due to the high density of states in these species, however, we argue that dissociation occurs as soon as the ground separated atom limit is exceeded. Based on this argument, the measured predissociation thresholds are assigned as the BDEs of the corresponding molecules.

These measurements provide fundamental information about the chemical bonding in this series of molecules, and have been combined with other quantities to obtain enthalpies of formation of the gaseous MSi molecules and ionization energies of the CoSi and NiSi molecules. It is our hope that the precise BDE values obtained in this study will serve as benchmarks for the further development of quantum chemical methods that may be reliably used to calculate the problematic transition metal species.

[1] A. E. Kramida, Y. Ralchenko, J. Reader, and a. N. A. Team, *NIST Atomic Spectra Database, version 5.4* (National Institute of Standards and Technology, Gaithersburg, MD, 2017).

[2] H. Hotop and W. C. Lineberger, J. Phys. Chem. Ref. Data **14**, 731–750 (1985).

[3] B. S. Freiser, Understanding Chem. React. **15**, 283–332 (1996).

[4] P. B. Armentrout and B. L. Kickel, Understanding Chem. React. **15**, 1–45 (1996).

[5] P. B. Armentrout, Top. Organomet. Chem. **4**, 1–45 (1999).

[6] P. B. Armentrout, Int. J. Mass Spectrom. **227**, 289–302 (2003).

[7] R. A. VanGundy, J. H. Bartlett, and M. C. Heaven, J. Mol. Spectrosc. **344**, 17–20 (2018).

[8] R. A. Van Gundy, J. H. Bartlett, M. C. Heaven, S. R. Battey, and K. A. Peterson, J. Chem. Phys. **146**, 054307 (2017).

[9] Z. Luo, Y.-C. Chang, Z. Zhang, and C. Y. Ng, Mol. Phys. **113**, 2228–2242 (2015).

[10] Z. Luo, Y.-C. Chang, Y. Pan, K.-C. Lau, and C. Y. Ng, J. Phys. Chem. A **120**, 4643–4654 (2015).

[11] J. H. Bartlett, I. O. Antonov, and M. C. Heaven, J. Phys. Chem. A **117**, 12042–12048 (2013).

[12] K. D. D. Gunaratne, C. Berkdemir, C. L. Harmon, and A. W. Castleman, Phys. Chem. Chem. Phys. **15**, 6068–6079 (2013).

[13] J. B. Kim, M. L. Weichman, and D. M. Neumark, J. Chem. Theory Comput. **10**, 5235–5237 (2014).

[14] G. Aravind, M. Nrisimhamurty, R. G. Mane, A. K. Gupta, and E. Krishnakumar, Phys. Rev. A **92**, 042503 (2015).

[15] Q.-Y. Liu, L. Hu, Z.-Y. Li, C.-G. Ning, J.-B. Ma, H. Chen, and S.-G. He, J. Chem. Phys. **142**, 164301 (2015).

[16] J. O. Kafader, M. Ray, and C. C. Jarrold, J. Chem. Phys. **143**, 034305 (2015).

[17] E. M. Spain and M. D. Morse, Int. J. Mass Spectrom. Ion Processes **102**, 183–197 (1990).

[18] E. M. Spain and M. D. Morse, J. Phys. Chem. **96**, 2479–2486 (1992).

[19] L. M. Russon, S. A. Heidecke, M. K. Birke, J. Conceicao, M. D. Morse, and P. B. Armentrout, J. Chem. Phys. **100**, 4747–4755 (1994).

[20] A. M. James, P. Kowalczyk, E. Langlois, M. D. Campbell, A. Ogawa, and B. Simard, J. Chem. Phys. **101**, 4485–4495 (1994).

[21] D. S. Yang, A. M. James, D. M. Rayner, and P. A. Hackett, J. Chem. Phys. **102**, 3129–3134 (1995).

[22] N. J. DeYonker, K. A. Peterson, G. Steyl, A. K. Wilson, and T. R. Cundari, J. Phys. Chem. A **111**, 11269–11277 (2007).

[23] M. L. Laury and A. K. Wilson, J. Chem. Theory Comput. **9**, 3939–3946 (2013).

[24] S. Luo, B. Averkiev, K. R. Yang, X. Xu, and D. G. Truhlar, J. Chem. Theory Comput. **10**, 102–121 (2014).

[25] W. Zhang, D. G. Truhlar, and M. Tang, J. Chem. Theory Comput. **10**, 2399–2409 (2014).

[26] S. Manivasagam, M. L. Laury, and A. K. Wilson, J. Phys. Chem. A **119**, 6867–6874 (2015).

[27] J. Wang, S. Manivasagam, and A. K. Wilson, J. Chem. Theory Comput. **11**, 5865–5872 (2015).

[28] S. Grimmel, G. Schoendorff, and A. K. Wilson, J. Chem. Theory Comput. **12**, 1259–1266 (2016).

[29] H. S. Yu, X. He, and D. G. Truhlar, J. Chem. Theory Comput. **12**, 1280–1293 (2016).

[30] J. L. Bao, X. Zhang, X.-F. Xu, and D. G. Truhlar, Phys. Chem. Chem. Phys. **19**, 5839–5854 (2017).

[31] Y. A. Aoto, A. P. de Lima Batista, A. Köhn, and A. G. S. de Oliveira-Filho, J. Chem. Theory Comput. **13**, 5291–5316 (2017).

[32] Y.-R. Luo, *Comprehensive Handbook of Chemical Bond Energies* (CRC Press, Taylor and Francis Group, Boca Raton, 2007).

[33] J. Drowart, C. Chatillon, J. Hastie, D. Bonnell, M. A. Alairo Franco, C. B. Alcock, O. L. Alves, A. M. Anthony, M. B. Badri, G. Balducci, E. J. Baran, J. F. Baumard, G. Bayer, H. P. Boehm, R. J. Brook, J. O. Carlsson, A. V. Chadwick, C. B. J. Chatillon, J. H. Choy, J. B. Clark, J. Corish, F. M. Costa, J. P. Coutures, G. De Maria, D. de Waal, M. Drabik, J. D. Drowart, P. Echegut, J. G. Edwards, M. S. E. El-Sewefy, P. Ettmayer, E. Fitzer, P. W. Gilles, J. Gopalakrishnan, L. N. Gorokhov, G. P. Grieveson, L. V. Gurvich, F. Hanic, J. W. Hastic, H. Hausner, M. G. Hocking, D. Holland, B. G. Hyde, M. Jafelicci, Jr., L. Kihlborg, C. H. Kim, M. Kizilyalli, R. Kniep, D. Kolar, K. L. Komarek, K. Koumoto, M. Leskela, M. H. Lewis, C. M. Lieber, J. Livage, B. Lux, K. J. D. MacKenzie, A. Magneli, C. K. Mathews, J. Matousek, H. J. Matzke, E. R. McCartney, R. Metselaar, J. Mintmire, A. Mocellin, S. Mrowee, W. L. Ng, M. Nygren, R. W. Ohse, P. Peshev, G. Petzow, M. H. Rand, M. M. Ristic, G. M. Rosenblatt, P. Saha, T. Saito, T. Sata, R. Sersale, F. Solymosi, S. Somiya, K. E. Spear, G. V. Subba Rao, A. P. B. Sinha, M. Thackeray, L. Tichy, R. J. D. Tilley, G. Van Tendeloo, R. Vernerkar, H. Verweij, G. F. Voronin, N. E. Walso de Reca, W. L. Worrell, D. S. Yan, H. Yanagida, T. S. Yen, and J. J. Ziokowski, Pure Appl. Chem. **77**, 683–737 (2005).

[34] A. V. Auwera-Mahieu, N. S. McIntyre, and J. Drowart, Chem. Phys. Lett. **4**, 198–200 (1969).

[35] A. Vander Auwera-Mahieu, R. Peeters, N. S. McIntyre, and J. Drowart, Trans. Faraday Soc. **66**, 809–816 (1970).

[36] E. L. Johnson, Q. C. Davis, and M. D. Morse, J. Chem. Phys. **144**, 234306 (2016).

[37] S. Taylor, E. M. Spain, and M. D. Morse, J. Chem. Phys. **92**, 2698–2709 (1990).

[38] J. M. Behm, C. A. Arrington, and M. D. Morse, J. Chem. Phys. **99**, 6409–6415 (1993).

[39] C. A. Arrington, T. Blume, M. D. Morse, M. Doverstål, and U. Sassenberg, J. Phys. Chem. **98**, 1398–1406 (1994).

[40] J. M. Behm, D. J. Brugh, and M. D. Morse, J. Chem. Phys. **101**, 6487–6499 (1994).

[41] J. D. Langenberg and M. D. Morse, Chem. Phys. Lett. **239**, 25–30 (1995).

[42] Z. Fu, L. M. Russon, M. D. Morse, and P. B. Armentrout, Int. J. Mass Spectrom. **204**, 143–157 (2001).

[43] J. J. Sorensen, T. D. Persinger, A. Sevy, J. A. Franchina, E. L. Johnson, and M. D. Morse, J. Chem. Phys. **145**, 214308 (2016).

[44] D. J. Matthew, E. Tieu, and M. D. Morse, J. Chem. Phys. **146**, 144310 (2017).

[45] A. Sevy, R. F. Huffaker, and M. D. Morse, J. Phys. Chem. A **121**, 9446–9457 (2017).

[46] A. Sevy, J. J. Sorensen, T. D. Persinger, J. A. Franchina, E. L. Johnson, and M. D. Morse, J. Chem. Phys. **147**, 084301 (2017).

[47] A. Sevy, D. J. Matthew, and M. D. Morse, J. Chem. Phys. **149**, 044306 (2018).

[48] A. Ferrarotti, H.-P. Gail, L. Degiorgi, and H. R. Ott, Astron. Astrophys. **357**, L13–L16 (2000).

[49] S. Tateno, Y. Kuwayama, K. Hirose, and Y. Ohishi, Earth Planet. Sci. Lett. **418**, 11–19 (2015).

[50] W. C. Wiley and I. H. McLaren, Rev. Sci. Instrum. **26**, 1150–1157 (1955).

[51] E. L. Johnson and M. D. Morse, J. Chem. Phys. **143**, 104303 (2015).

[52] J. B. Paul, J. J. Scherer, C. P. Collier, and R. J. Saykally, J. Chem. Phys. **104**, 2782–2788 (1996).

[53] L. Shao, S. M. Sickafoose, J. D. Langenberg, D. J. Brugh, and M. D. Morse, J. Chem. Phys. **112**, 4118–4123 (2000).

[54] E. Wigner and E. E. Witmer, Z. Phys. **51**, 859–886 (1928).

[55] G. Herzberg, *Molecular Spectra and Molecular Structure I. Spectra of Diatomic Molecules*, 2nd ed. (Van Nostrand Reinhold, New York, 1950).

[56] H. Lefebvre-Brion and R. W. Field, *The Spectra and Dynamics of Diatomic Molecules* (Elsevier, Amsterdam, 2004).

[57] M. Sekiya, K. Miwa, K. Tanaka, and M. Yoshimine, Mol. Phys. **101**, 99–104 (2003).

[58] Z. J. Wu and Z. M. Su, J. Chem. Phys. **124**, 184306 (2006).

[59] B. Suo, Y. Lian, W. Zou, and Y. Lei, J. Phys. Chem. A **122**, 5333–5341 (2018).

[60] N. Lindholm and M. D. Morse, J. Chem. Phys. **127**, 084317 (2007).

[61] A. G. Adam, A. D. Granger, W. J. Balfour, and R. Li, J. Mol. Spectrosc. **258**, 35–41 (2009).

[62] A. Le, T. C. Steimle, M. D. Morse, M. A. Garcia, L. Cheng, and J. F. Stanton, J. Phys. Chem. A **117**, 13292–13302 (2013).

[63] M. A. Garcia, C. Vietz, F. Ruipérez, M. D. Morse, and I. Infante, J. Chem. Phys. **138**, 154306 (2013).

[64] N. F. Lindholm, D. J. Brugh, G. K. Rothschopf, S. M. Sickafoose, and M. D. Morse, J. Chem. Phys. **118**, 2190–2196 (2003).

[65] D. Tzeli and A. Mavridis, J. Chem. Phys. **126**, 194304 (2007).

[66] G. Schoendorff, A. R. Morris, E. D. Hu, and A. K. Wilson, J. Phys. Chem. A **119**, 9630–9635 (2015).

[67] I. Shim and K. A. Gingerich, Z. Phys. D: At., Mol. Clusters **12**, 373–376 (1989).

[68] H. Haberlandt, Chem. Phys. **138**, 315–325 (1989).

[69] I. Shim and K. A. Gingerich, Z. Phys. D: At., Mol. Clusters **16**, 141–148 (1990).

[70] M. Barysz and P. Pyykkö, Chem. Phys. Lett. **368**, 538–541 (2003).

[71] B. L. Kickel and P. B. Armentrout, J. Am. Chem. Soc. **116**, 10742–10750 (1994).

[72] B. L. Kickel and P. B. Armentrout, J. Am. Chem. Soc. **117**, 764–773 (1995).

[73] B. L. Kickel and P. B. Armentrout, J. Phys. Chem. **99**, 2024–2032 (1995).

[74] B. L. Kickel and P. B. Armentrout, J. Am. Chem. Soc. **117**, 4057–4070 (1995).

[75] S. A. Heidecke, Z. Fu, J. R. Colt, and M. D. Morse, J. Chem. Phys. **97**, 1692–1710 (1992).

[76] A. Martinez, N. Lindholm, and M. D. Morse, J. Chem. Phys. **135**, 134308 (2011).

[77] S. A. Cooke, M. C. L. Gerry, D. J. Brugh, and R. D. Suenram, J. Mol. Spectrosc. **223**, 185–194 (2004).

[78] M. W. Chase, Jr., *NIST-JANAF Thermochemical Tables*, 4th ed. (American Institute of Physics for the National Institute of Standards and Technology, Washington, D.C., 1998).

[79] L. V. Gurvich, G. V. Karachevtsev, V. N. Kondratyev, Y. Lebedev, V. A. Medvedev, V. Potapov, and S. Hodeev, *Bond Energies of Chemical Bonds, Ionization Potentials and Electron Affinities* (Nauka, Moscow, 1974).

[80] J. E. Kingcade, Jr. and K. A. Gingerich, J. Chem. Soc., Faraday Trans. 2 **85**, 195–200 (1989).

[81] M. Tomonari and K. Tanaka, Theor. Chem. Acc. **106**, 188–193 (2001).

[82] Y. M. Hamrick and W. Weltner, Jr., J. Chem. Phys. **94**, 3371–3380 (1991).

[83] Y. Lefebvre and J. Schamps, J. Mol. Spectrosc. **201**, 128–133 (2000).

[84] G. Riekert, P. Lamparter, and S. Steeb, Z. Metallkd. **72**, 765–768 (1981).

[85] J. E. Kingcade, Jr. and K. A. Gingerich, J. Chem. Phys. **84**, 4574–4578 (1986).

[86] I. Shim, J. E. Kingcade, and K. A. Gingerich, Z. Phys. D: At., Mol. Clusters **7**, 261–269 (1987).

[87] P. Turski and M. Barysz, J. Chem. Phys. **113**, 4654–4661 (2000).

[88] M. Abe, T. Nakajima, and K. Hirao, J. Chem. Phys. **117**, 7960–7967 (2002).

[89] K. A. Gingerich, R. Haque, and J. E. Kingcade, Jr., Thermochim. Acta **30**, 61–71 (1979).